Magnetic properties and critical currents in Tl-based high-T_c superconducting single crystals

G. Brandstätter, F. M. Sauerzopf, and H. W. Weber
Atominstitut der Österreichischen Universitäten, A-1020 Wien, Austria
(Received 16 December 1996)

$Tl_2Ca_2Ba_2Cu_3O_{10}$ (Tl-2223) and $(TlPb)(SrBa)_2Ca_2Cu_3O_8$ (Tl-1223) single crystals were investigated by superconducting quantum interference device magnetometry in fields up to 8 T ($H\|c$ axis). The samples were subjected to sequential reactor neutron irradiation up to a fluence of 24×10^{21} m^{-2} ($E>0.1$ MeV). The superconducting transition temperature T_c, the magnetization, and the irreversibility lines were measured before and after each irradiation step. Because of the wide range of magnetic fields and temperatures, where the magnetization is totally reversible, especially in Tl-2223, the basic mixed-state parameters, such as the critical magnetic fields and the characteristic lengths, could be evaluated. In the irreversible range, the critical current densities were calculated from the hysteresis loops using an extended Bean model. We find that J_c is strongly enhanced by the radiation-induced defects, e.g., by a factor of 52 in Tl-2223 at 40 K and 1 T. The irreversibility lines are shifted to higher fields and temperatures, but remain always below those of unirradiated Tl-1223, even at the highest neutron fluence. In Tl-1223, the critical current densities are moderately enhanced. The irreversibility line is at the same position or even higher than that of Y-123 and is moderately shifted to higher fields and temperatures after irradiation. The experimental results are discussed in terms of flux pinning and dimensionality. [S0163-1829(97)03217-7]

I. INTRODUCTION

Since the discovery of superconductivity in LaBaCuO,[1] many other high-T_c oxide superconductors have been found. The family of Tl-based cuprate superconductors[2] consists of two subfamilies, which can be described by the general chemical formulas $TlCa_{n-1}Ba_2Cu_nO_{2n+3}$ for Tl-O single-layer and $Tl_2Ca_{n-1}Ba_2Cu_nO_{2n+4}$ for Tl-O double-layer compounds, with $n=1$, 2, or 3. Within each subfamily the number of CuO_2 planes can vary, which results in a large number of Tl-based superconductors with different properties and transition temperatures up to 125 K. They have a tetragonal structure at room temperature with lattice parameters $a=b$ and c. The monolayer compounds have primitive tetragonal unit cells, the bilayer compounds body-centered tetragonal unit cells. Therefore, twin boundaries are not formed. The c axis of the monolayer compounds is short, with a maximum of 1.5871 nm for the Tl-1223 structure, which leads to a more three-dimensional (3D) behavior in the superconducting state, similar to Y-123. In the bilayer compounds, the c axis is long, up to 3.5662 nm for the Tl-2223 structure. Because of the large distances between the CuO_2 planes, they show strongly 2D behavior. For practical applications, the critical current density J_c, especially at and above 77 K, is of major importance. Layered high-T_c superconductors show high J_c values comparable to or even higher than in conventional superconductors at low temperatures. The disadvantage, however, is that J_c is strongly temperature and field dependent and becomes negligible at relatively low temperatures compared to their transition temperature (above $\sim T_c/2$). One way of increasing flux pinning and thus J_c is to introduce defects such as columnar tracks or defect cascades in a controlled manner.[3] These defects act as strong pinning centers, even above 77 K. Fast neutrons produce so-called defect cascades consisting of highly disordered or amorphous material. In the case of Y-123, the mean diameter of the cascade is 2.5 nm and the surrounding strain field has about the same size, which results in a spherical defect volume with a diameter of about 5 nm.[4] Investigations of the defect structure in neutron-irradiated Bi-2212 single crystals led to similar results.[5] In this case, the cascades have diameters of 2–4 nm without the strain field. The defect concentration is $(3.7\pm1)\times10^{22}$ m^{-3} per 10^{22} neutrons/m^2 ($E>0.1$ MeV), somewhat smaller than in Y-123.[4] Therefore, we expect that similar defects should prevail in Tl-based oxide superconductors, since their elemental composition is similar to Y-123 or Bi-2212, but no actual information is available at present.

Single crystals of two Tl-based high-T_c superconducting compounds Tl-2223 and Tl-1223 were studied in the unirradiated as well as in the irradiated state. Their mixed-state properties as well as data on J_c, the irreversibility line, and T_c are presented in the following and compared to each other. The irreversible properties are discussed in terms of flux pinning and dimensionality.

II. EXPERIMENT

High-quality single crystals with nominal composition Tl-2223 and (TlPb)(SrBa)-1223 were grown according to the procedures outlined in Ref. 6. The Tl-2223 single crystals were small platelets with dimensions of 170–600 μm$\times$300–900 μm in the basal plane and 70–110 μm along the c axis. Several crystals from three different batches were available. The Tl-1223 single crystals have dimensions of 380–628 μm$\times$350–426 μm in the basal plane and 108–213 μm along the c axis. Single crystals from only one batch were available. All investigations were carried out in a 1-T as well as in an 8-T superconducting quantum interference device (SQUID) magnetometer. The single crystals were mounted onto small U-shaped aluminum sample holders, which allow an accurate and reproducible orientation with respect to the

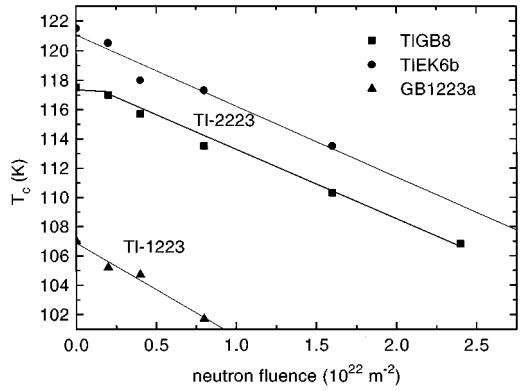

FIG. 1. T_c as a function of fluence for Tl-2223 and Tl-1223 single crystals.

field. The U-shaped holders were then inserted into an aluminum rod. The orientation of the c axis was always kept parallel to the applied field. Only the transition temperatures were measured with the c axis perpendicular to the field (1.1 mT). J_c was calculated from hysteresis loops measured in fields up to 8 T at several fixed temperatures (5, 10, 20, 30, 40, 50, 60, 77, and 93 K). The irreversibility lines and the reversible mixed-state properties were determined from zero-field-cooled (ZFC) and field cooled (FC) curves measured between 10 K and temperatures above T_c, in several fixed fields. All measurements were carried out in the unirradiated state as well as after each irradiation step.

The samples were irradiated in the central core position of the 250-kW TRIGA reactor in Vienna, the flux density distribution of which has been established accurately.[7] At full reactor power, the flux density of fast neutrons amounts to 7.6×10^{16} m^{-2} s^{-2} ($E>0.1$ MeV). The samples were encapsulated in small quartz tubes which were back filled with helium. During the irradiation process, the tube was contained in a small open aluminum can immersed in the cooling water of the reactor. The temperature during irradiation is not well known, but estimated to be below 60 °C. The single crystals were subjected to fluences of 2×10^{21}, 4×10^{21}, 8×10^{21}, and 16×10^{21} m^{-2}. One sample (TlGB8) was also subjected to a fluence of 24×10^{21} m^{-2}.

III. RESULTS AND DISCUSSION

A. Transition temperature T_c

A fit of the FC curve near the transition to $m_{\rm FC}(T)=a\{1-\exp[(T-T_c)/b]\}$, with fit parameters T_c, a, and b provides us with an accurate and reproducible estimation of the transition temperature T_c. The Tl-2223 single crystals had the highest T_c, between 117.5 K and up to 121.5 K, but still somewhat lower than found for ceramics [up to 125 K (Ref. 8)]. Tl-1223 has, in general, a slightly lower T_c [116-120 K in ceramics (Ref. 9)], but the T_c of our crystals was considerably lower (107 K).

With irradiation, T_c decreases in both materials continuously (Fig. 1). For the Tl-2223 single crystals, T_c shows a small plateau at the lowest fluence (the difference between the transition temperatures before and after the first irradiation step is less than 1 K), but then generally a linear decrease with a slope of -4.4 to -4.8 K per 10^{22} neutrons/m^2. This decrease is more pronounced than in Y-123 (-1.74 K per 10^{22} neutrons/m^2).[10] Because of the higher initial T_c of Tl-2223, T_c would reach 0 K at a fluence of 3×10^{23} neutrons/m^2, which is almost 3 times higher than for Y-123. The decrease of T_c with increasing neutron fluence is almost linear in Tl-1223 with a slope of -6.4 K per 10^{22} neutrons/m^2, i.e., stronger than in Tl-2223. In addition, the small plateau at low fluences is not found for this material.

T_c, defined as above by the diamagnetic onset, might be influenced by thermally activated vortex fluctuations and thus be underestimated. Extrapolation of $H_{c2}(T)$ and $\lambda_{ab}^{-2}(T)$ to zero leads to a mean-field transition temperature $T_c^{\rm MF}$, which is several K higher.[11] However, quantities such as the penetration depth are not accessible to a magnetization experiment; i.e., they must be deduced from $M(T)$ measurements using theory (e.g., Ref. 12). Therefore, defining T_c by the diamagnetic onset is the most reliable procedure at present and used throughout this work. The variation of T_c among crystals of the same material is attributed to different as-grown defect structures. The small plateau at low fluences is similar to that found in Y-123.[10] The plateau and the decrease of T_c can be explained by a simple model,[10] which is based on the disorder introduced during the irradiation process. Oxygen atoms emitted during the creation of defect cascades move through the crystal and can recombine with oxygen-deficient point defects. Thus the total number of defects might be reduced, leaving the total order unchanged or even slightly improved. At high fluences the number of cascades and of less-mobile defects rapidly increases, thus decreasing T_c. Crystals of lower quality already have large defects acting as defect sinks for point defects in the as-grown state, which are quickly saturated. Therefore, the plateau is smaller and the decrease of T_c is stronger. Since the general character of superconductivity is the same as in Y-123, this model should also apply to the Tl-2223 and Tl-1223 crystals. Because of the nearly equal slopes (TlEK6b, TlGB8), the difference in T_c can only be caused by the as-grown defect structure, indicating that TlGB8 is of less quality than TlEK6b. The low T_c of the Tl-1223 single crystal might arise partly from the as-grown defect structure and partly because of oxygen overdoping.[13] Annealing of Tl-1223 single crystals in Ar showed an increase of T_c.[13]

B. Reversible mixed-state properties

Because of weak flux pinning in ''two-dimensional'' high-temperature superconductors, large sections of the H,T phase diagram are accessible to an investigation of the reversible mixed-state properties. However, conventional models, such as Ginzburg-Landau (GL) and London theory, are not applicable[14] because of the reduced dimensionality of these materials and because of thermally induced fluctuations. Recent theoretical work[15,16] led to the development of models applicable to 2D systems, which take these fluctuations into account. We analyzed our data using the model described in Ref. 16, because it is simple and does not require complicated calculations. The model developed by Koshelev[15] might have a better theoretical background, but one quantity necessary for the evaluation of the reversible mixed-state parameters is not yet available.

Several groups used the model developed by Bulaevskii *et al.*[16] They tried to extract the interlayer distance s from the

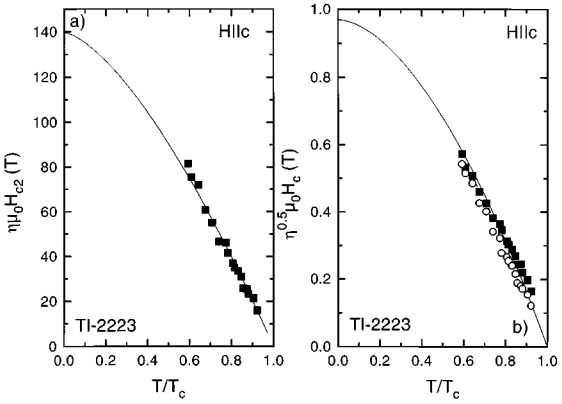

FIG. 2. Temperature dependence of the upper critical field. The solid line is a fit to the BCS relation. Temperature dependence of the thermodynamic critical field. The solid line is a fit to the BCS relation.

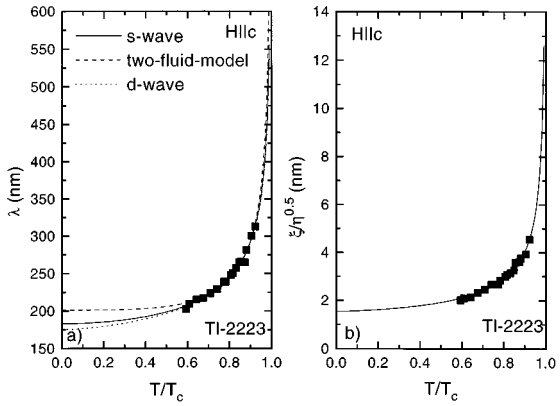

FIG. 3. Temperature dependence of the penetration depth. Temperature dependence of the coherence length.

crossing point magnetization $(T^*, \mu_0 M^*)$, which is based on the assumption that the factor $\ln(\alpha\eta/\sqrt{e})$ is equal to unity. The resulting s was then too large (by a factor of about 3). This was explained by nonsuperconducting inclusions, which might be reasonable for polycrystalline ceramics, but is definitely not adequate for single crystals. Here we start our calculations in the opposite way. The crossing point magnetization is given by

$$\mu_0 M^* = -\frac{\mu_0 k_B T^*}{s\Phi_0} \ln\frac{\alpha\eta}{\sqrt{e}}. \tag{1}$$

The crystallographic interlayer distance s is 1.8 nm for Tl-2223, and M^* and T^* are known from the FC curves. We obtain 0.4094 for $\ln\alpha\eta/\sqrt{e}$. The penetration depth $\lambda(T)$ is independent of η/e:

$$\frac{\partial\mu_0 M}{\partial \ln\mu_0 H} = \frac{\Phi_0}{8\pi\lambda^2}[1-g(T)], \tag{2}$$

with $g(T)=8\pi\lambda^2\mu_0 k_B T/\phi_0^2 s$. The equation for H_{c2} is significantly changed, since an additional term has to be considered:

$$\ln\frac{\eta H_{c2}}{eH} = \frac{1}{1-g}\left[g\left(\ln g - \ln\frac{\alpha\eta}{\sqrt{e}}\right) - \frac{8\pi\lambda^2}{\Phi_0}\mu_0 M\right]. \tag{3}$$

It is not so important to know α, but η is essential. This model is only valid if $\phi_0^2 s/8\mu_0 k_B T\lambda^2 \geqslant \ln\lambda_J^2 B/\phi_0$. With $\lambda_J = 100$–5000 nm,[17] we are restricted to temperatures $t=T/T_c=0.9$–0.98. Quantum fluctuations becoming apparent at low fields and low temperatures and leading to marked deviations of $\partial M/\partial \ln H$ from linearity[18] were not taken into account, since we refer only to high temperatures ($T>70$ K), where they do not contribute to the free energy significantly.[19] Figure 2(a) shows the temperature dependence of $\eta\mu_0 H_{c2}$ of TlEK6b, which was analyzed in terms of the BCS clean limit theory using the normalized function $h_{c2}=-H_{c2}/T_c(dH_{c2}/dT)_{T_c}$.[20] At first, the numerical BCS data were fitted to obtain an approximate theoretical temperature dependence, which turns out to be $(1-t^{3/2})$. Hence the experimental data were fitted to $\eta\mu_0 H_{c2}(0)(1-t^{3/2})$ with the fit parameter $\eta\mu_0 H_{c2}(0)$. The fit is excellent and results in $\eta\mu_0 H_{c2}(0)\approx 140$ T.

$\lambda_{ab}(T)$ was fitted to the expression $\lambda_0(1-t^2)^{-a}$ [Fig. 3(a)], which follows from the best fit to the BCS clean limit data tabulated by Mühlschlegel[21] with $a=0.5$. Here $\lambda(0)$ and a are fit parameters. As demonstrated in Fig. 3(a), the data can be fitted with $\lambda_0=183$ nm and $a=0.28$, but the exponent a deviates severely from the original BCS value ($a=0.5$). A fit to the two-fluid model $\lambda_0(1-t^4)^{-b}$ ($b=0.36$, $\lambda_0=201$ nm) and to the best fit to the d-wave model, $\lambda_0(1-t^{1.5})^{-c}$ ($c=0.27$, $\lambda_0=175$ nm) yields similar results. Here b and c should also be 0.5. It is not possible to finally decide between these temperature dependences, because of two reasons: First, the main differences occur for $t<0.5$, where no data are available. Second, the exponent deviates severely from 0.5 in all cases. This may be a consequence of the evaluation process, which requires a linear fit of the reversible $M(T)$ region. A more sophisticated theoretical treatment (e.g., Ref. 12) may result in an exponent closer to the original value of 0.5, since the actual curvature and thus the actual slope of $M(T)$ are used for the calculation of $\lambda(T)$.

From the GL expression $\eta\mu_0 H_{c2}=\phi_0\eta/2\pi\xi^2$, the coherence length ξ is calculated. Based upon the temperature dependence of the upper critical field, we get $\xi/\sqrt{\eta}(1-t^{1.5})^{-0.5}$. The expression fits the data well, leading to $\xi(0)/\sqrt{\eta}\approx 1.54$ nm, which is consistent with the result obtained from $\eta\mu_0 H_{c2}(0)$ directly.

The GL parameter κ is given by λ/ξ and calculated from the above data. Here $\kappa\sqrt{\eta}$ is weakly temperature dependent with an average value of about 83. Finally, the thermodynamic critical field is calculated from the GL relation $\sqrt{\eta}H_c=\phi_0\sqrt{\eta}/2\sqrt{2}\pi\mu_0\lambda\xi$ as well as by integration of the reversible magnetization curve from 0 to $\eta\mu_0 H_{c2}$. The resulting data do not differ very much. Figure 2(b) shows the temperature dependence of $\sqrt{\eta}\mu_0 H_c$. It can be fitted best to the BCS clean limit data given by Mühlschlegel,[21] $\sqrt{\eta}\mu_0 H_c(0)(1-t^{7/4})$. The result is $\sqrt{\eta}\mu_0 H_c\approx 0.968$ T. For the slope of H_c at T_c, we get -13.9 mT/K. Using the κ value given above and the relation $\kappa\sqrt{2}H_c'(T_c)=H_{c2}'(T_c)$, we find for $\eta\mu_0 H_{c2}'(T_c)=-1.64$ T/K, which agrees well with that calculated from $\eta\mu_0 H_{c2}(T_c)$ directly (-1.73 T/K).

Finally, we wish to retrieve absolute values for the above

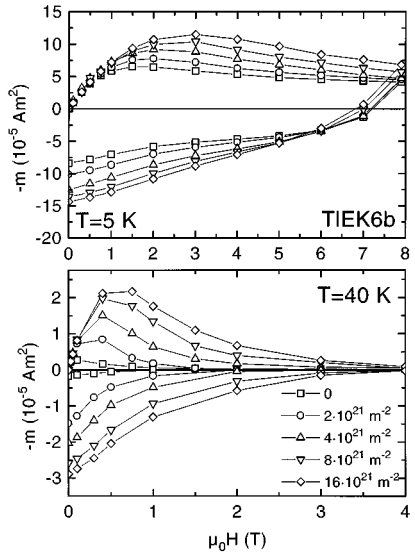

FIG. 4. Magnetization curves of Tl-2223 at different temperatures.

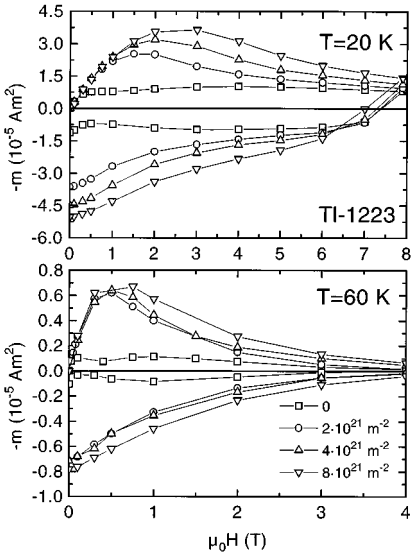

FIG. 5. Magnetization curves of Tl-1223 at different temperatures.

quantities at 0 K. According to Koshelev,[15] $\eta \approx 0.95$, which then leads to $\mu_0 H_{c2}(0) \approx 147$ T, $\xi(0) \approx 1.5$ nm, $\kappa \approx 85$, and $\mu_0 H_c(0) \approx 0.993$ T. In order to check the validity of these evaluation procedures, a simple thermodynamic relation

$$\frac{\Delta c}{T_c} = V\left(\frac{dB_c}{dT}\right)^2\Bigg|_{T_c} \tag{4}$$

is used to find the specific heat jump at T_c, which can be compared to experiment. From Eq. (4), $\Delta c/T_c$ normalized to 1 mol is 31 mJ/K^2, which is somewhat higher than reported by Junod *et al.* [14 mJ/K^2 mol (Ref. 22)]. This difference may be due to the fact that we actually do not really know the slope at the transition, we simply assumed that the slope close to the transition does not change with increasing temperature. However, recent experimental work suggested that the slope might actually become zero due to the fluctuations, thus giving no jump in the specific heat.[23] A similar analysis of the reversible magnetization data in the irradiated state (16×10^{21} m^{-2}) leads to $\lambda_0 = 255$ nm (exponent $a = 0.17$), $\mu_0 H_{c2}(0) \approx 220$ T, $\xi(0) \approx 1.22$ nm, $\kappa \approx 124$, and $\mu_0 H_c(0) \approx 0.967$ T. These results will be used for the calculation of the condensation energy of a pancake pinned by different defects in the next section.

C. J_c and irreversibility lines

The critical current densities were calculated as a function of the local induction from the hysteresis loops (Figs. 4 and 5) using an extended Bean model,[24] which takes demagnetization effects into account. In the unirradiated state, the J_c's of several Tl-2223 single crystals and of one Tl-1223 single crystal were determined. We found a large sample-to-sample variation of J_c within one and the same compound: J_c^{ab} ranges from $\sim 1\times10^{10}$ A m^{-2} (TlGB8) to $\sim 3\times10^{10}$ A m^{-2} (TlEK6b) below 1 T at 5 K. These values are equal to or slightly higher than those found in Y-123 single crystals.[25] Here J_c of Tl-2223 is strongly temperature and field dependent and disappears already above 40 K (see Fig. 6). Almost completely reversible magnetization loops were found at 60 K. Figure 7 summarizes J_c in Tl-1223 at different temperatures. A striking feature is the existence of fishtails.[26] They are already pronounced at 10 K and found up to 77 K. At lower temperatures they keep J_c nearly constant up to 8 T; e.g., at 10 K, $J_c = 2.3\times10^{10}$ A m^{-2} over the entire induction range. Although J_c in Tl-1223 and Tl-2223 are nearly equal at low temperatures and low inductions (at 10 K and 1 T about 2.5×10^{10} A m^{-2}), there is an enormous difference at high temperatures. At 1 T and 40 K, J_c in Tl-1223 is about one order of magnitude larger. At higher inductions, J_c is zero in Tl-2223. Because of the fishtails, the field and temperature dependence of J_c in Tl-1223 is not as strong as in the related double-layer material. Here J_c drops below 10^9 A m^{-2} only above 60 K and is still 2×10^8 A m^{-2} at 77 K and 0.5 T. (Additional experiments on polycrystalline Tl-1223 confirmed these high intragrain critical current densities; i.e., J_c is 10^{11} A m^{-2} at 5 K and 4 T, and still about 10^8 A m^{-2} below 0.5 T at 93 K.)

Measurements with $H \| ab$ were carried out only on the Tl-1223 single crystal, since it has a considerably lower anisotropy factor (10–20) as estimated from the reversible properties. Here J_c^c is about one order of magnitude smaller

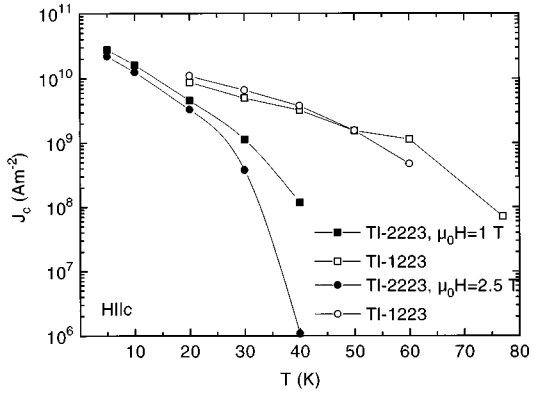

FIG. 6. J_c as a function of temperature for two different fields.

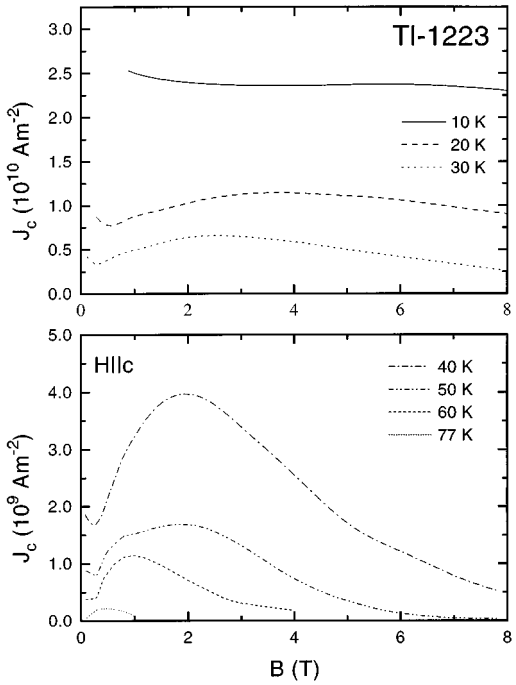

FIG. 7. J_c of unirradiated Tl-1223 at different fixed temperatures.

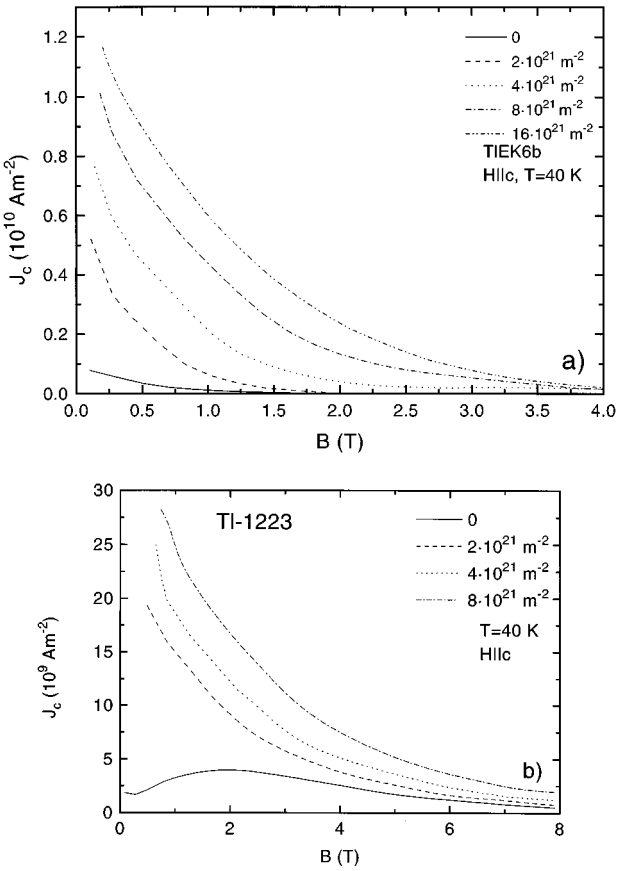

FIG. 8. J_c of Tl-2223 at 40 K before and after each irradiation step. J_c of Tl-1223 at 40 K before and after each irradiation step.

than for J_c^{ab} ($H\|c$) at all temperatures. For example, at 40 K and 1 T, J_c^c is about 1.9×10^8 A m^{-2}. A misorientation of the sample with respect to the field by about 1° might be possible, which could lead to a contribution of the c-axis moment. Thus, J_c^c might even be smaller for $H\|ab$.

Neutron irradiation of the single crystals to cumulative fluences up to 16×10^{21} m^{-2} results in a continuous increase in J_c after each step. TlGB8 was also subjected to 24×10^{21} m^{-2}, but J_c was then found to decrease at all temperatures and fields. Figure 8 shows J_c versus B data of Tl-2223 and Tl-1223 single crystals at 40 K.

In TlGB8, the increase at low temperatures is moderate, e.g., at 1 T and 5 K from 10^{10} to 2.1×10^{10} A m^{-2}; i.e., the enhancement factor is 2.1. However, at high temperatures, the increase is stronger; at 40 K and 1 T, J_c changes from zero to 1.3×10^9 A m^{-2}. A similar behavior is observed for TlEK6b [Fig. 8(a)]. Here J_c at 1 T and 5 K changes from 2.7×10^{10} to $5–6\times10^{10}$ A m^{-2} after the last irradiation step. At 40 K and 1 T the increase is much more pronounced, from 1.2×10^8 to 6.1×10^9 A m^{-2}, corresponding to an enhancement factor of 52. At 77 K, where $J_c(B)$ was zero in the unirradiated state, critical current densities of up to 6×10^8 A m^{-2} were found for $B<0.3$ T (cf. also the discussion of the irreversibility line).

Neutron irradiation of the Tl-1223 single crystal led to similar results [Fig. 8(b)]. The fishtails disappeared after the first irradiation step, leading to a strong enhancement at low and high inductions, respectively. The pinning mechanism responsible for the fishtails is masked by the newly induced defects, which act as strong pinning centers. Here J_c at 77 K and 0.5 T increased from 2.18×10^8 A m^{-2} (unirradiated) to 1.4×10^9 A m^{-2} (2×10^{21} m^{-2}), 1.9×10^9 A m^{-2} (4×10^{21} m^{-2}), and finally 2.15×10^9 A m^{-2} (8×10^{21} m^{-2}). A similar behavior is found at lower temperatures. At 40 K and 1 T, J_c increased from 3.22×10^9 A m^{-2} (unirradiated) to 2.5×10^{10} A m^{-2} (8×10^{21} m^{-2}). Even at 93 K, J_c values of up to 3×10^8 A m^{-2} are found below 0.2 T after the last step. At this temperature, J_c was zero before irradiation.

The irreversibility line was determined based upon the fact that the slow movement of a sample between pickup coils in a slightly inhomogeneous field is equivalent to the superposition of a small ripple field onto the applied dc field.[27] The ripple field is about 0.1% of the applied field at a ''frequency'' of 0.05 Hz.[28] As long as the sample is in the reversible regime, the SQUID response is symmetric. When the superconductor gets hysteretic, the ac field distorts the response curves, which can be seen immediately. Thus a very accurate determination of the irreversibility point, depending on the temperature step distance, is possible. In our case the irreversibility point was determined with an accuracy of ±1 K.

Results for $\mu_0 H_{\rm irr}$ as a function of the reduced temperature $t=T/T_c$ are plotted in Fig. 9. The reversible regime of Tl-2223 is very large and extends to almost $t=0.5$. This leads to a very small initial slope of the irreversibility line, which rapidly rises only at $t=0.3$. Although Tl-1223 is more three dimensional, the shape of its irreversibility line is more related to that of Tl-2223 than to that of Y-123. The tail with the very small and much shorter initial slope has not been found in any irreversibility line of Y-123. In all cases the form of the irreversibility line is better described by an exponential law than by a power law. Experimental data were fitted to $\mu_0 H_{\rm irr}(t)=b\exp(-at)$ with fitting parameters a and b.

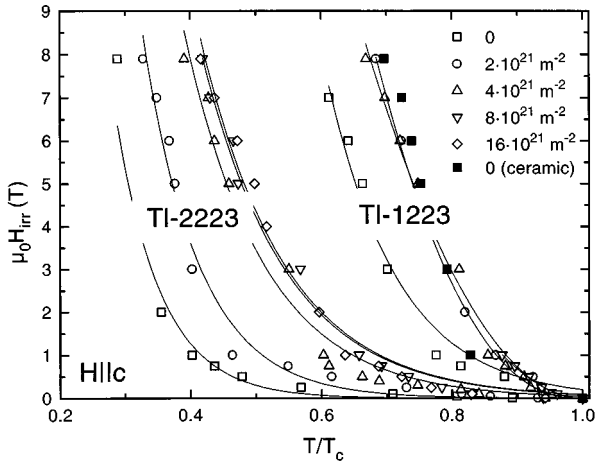

FIG. 9. Irreversibility lines for Tl-2223 and Tl-1223 before and after each irradiation step. The solid symbols mark the irreversibility line of polycrystalline Tl-1223.

After each irradiation step the irreversibility lines of the Tl-2223 and Tl-1223 single crystals shift to higher fields and temperatures (Fig. 9). The Tl-2223 irreversibility lines always follow the exponential law. However, in Tl-1223 a change from an exponential to a power law behavior is observed after the first irradiation step.

For TlEK6b the irreversibility lines at 8×10^{21} and 16×10^{21} m^{-2} are nearly identical (Fig. 9), whereas there is still a large difference between these two lines for the crystal TlGB8 [Fig. 10(a)]. However, the irreversibility line at 16×10^{21} m^{-2} of TlGB8 does not reach that of TlEK6b below 6 T [see Fig. 10(b)]. At the highest fluence (24×10^{21} m^{-2}), the irreversibility line drops below the previous one at about 3 T and $t=0.5$, indicating that a ''limiting'' fluence has already been trespassed, but there is still some further enhancement at low fields and higher temperatures [Fig. 10(a)]. Compared to the irreversibility line of Tl-1223 in the unirradiated state, the irreversibility lines of irradiated Tl-2223 are still much lower.

Neutron irradiation of the Tl-1223 single crystal has led to similar shifts. After the first step (2×10^{21} m^{-2}), the irreversibility line is shifted to higher fields and temperatures. After all other steps (up to 8×10^{21} m^{-2}), no further changes are observed within experimental uncertainty. Thus the increase of the irreversible regime is much more moderate than in Tl-2223. Because of the small signal at fields above 1 T, no irreversibility point for higher fields could be determined after the last irradiation step. The irreversibility line of an unirradiated bulk Tl-1223 sample is added in Fig. 9 (solid symbols) for comparison. After irradiation to a fluence of 2×10^{21} m^{-2}, this line remained at almost the same position. Thus the data suggest that this position is the highest that can be achieved for Tl-1223 by neutron irradiation.

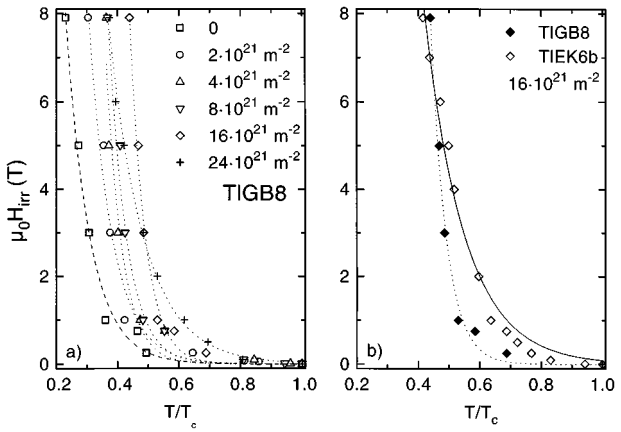

FIG. 10. Irreversibility lines for Tl-2223 (sample TlGB8) after sequential irradiation to fluences up to 24×10^{21} m^{-2}.

The low-lying irreversibility line and the rapid decrease of J_c with temperature are consequences of the layered structure of Tl-2223. At low temperatures, the magnetic microstructure consists of correlated stacks of pancakes. Because of their magnetic interaction, they are coupled and behave more or less like ordinary flux lines. They decouple at higher temperatures, and each pancake must be pinned individually, in contrast to the 3D case. In addition, the as-grown pinning centers become ineffective at high temperatures, which makes current flow without dissipation impossible. The situation in Tl-1223 is more like in Y-123, which leads to a more 3D behavior. Effective pinning is possible up to almost $t=0.8$, where the slope of the irreversibility line suddenly gets very flat. The shape of the irreversibility line of both compounds suggests the existence of different pinning mechanisms, one being dominant at low temperatures, the other being present over the entire temperature range and becoming dominant at high temperatures. Investigations of the flux dynamics, J_c, the normalized relaxation rate, and the irreversibility line by Metlushko *et al.*[29] actually led to the identification of three pinning regimes within the framework of the collective pinning theory for Tl-2223 superconductors.

After irradiation the pinning behavior remains nearly unchanged in both compounds at low temperatures, but alters tremendously at higher temperatures in Tl-2223. Figure 11(a) shows the temperature dependence of the enhancement factor $n=J_c/J_c^{\mathrm{unirr}}$. At 5 K and 1 T, no strong enhancement can be observed, $n<3$, whereas, at 40 K and 1 T, $n=52$ after the last irradiation step. At 77 K the increase is much more dramatic, since there was no J_c in the unirradiated state. A similar behavior occurs at higher fields. At low temperatures, the original defect structure seems to provide sufficiently strong pinning and the newly created defect cascades do not contribute much. This is reflected by the barely increasing enhancement factor. At 40 K, where J_c was already small in the as-grown sample, the increase is very high, $n=52$. This occurs at a temperature where the correlated stacks of pancakes should already have decoupled (as evidenced by the irreversibility line and the vanishing J_c in the unirradiated state). This strong increase then indicates that defect cascades are strong pinning centers even for pancakes. They pin the pancakes over a wide temperature range (up to $t=0.5$) after irradiation to a fluence of 16×10^{21} m^{-2}, since J_c is still increasing and reaching finite values even in a region, where the preirradiation values were equal to zero. The situation is different for Tl-1223. Here $n(T)$ shows a complicated structure due to the fishtails in the unirradiated state [Fig. 11(b)] and is about 10 or less at all temperatures, clearly smaller than for Tl-2223 irradiated to the same fluence (up to 35).

If J_c at a fixed field and temperature is plotted as a function of the fluence (Fig. 12), the maximum fluence the Tl-

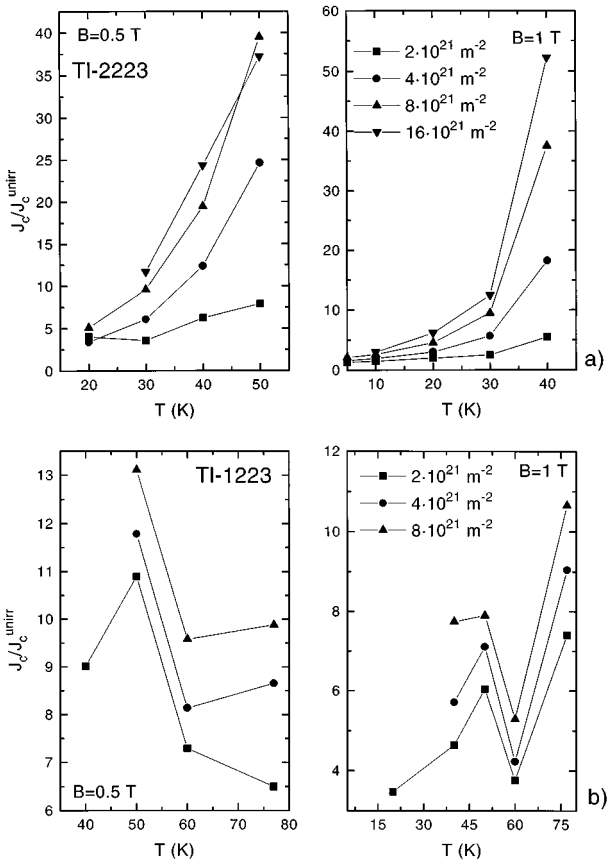

FIG. 11. Enhancement factors of the critical current density in Tl-2223 at 0.5 and 1 T. Enhancement factors for Tl-1223 at 0.5 and 1 T.

2223 crystal can sustain without major degradation of the superconducting properties seems to be 16×10^{21} m^{-2}. Here TlGB8 shows a drop of J_c at 24×10^{21} m^{-2}. All $J_c(B)$ curves fall below those at 16×10^{21} m^{-2}. This might be explained partly by the strong decrease of T_c after the last irradiation step [$T_c^{\rm unirr}-T_c(24\times10^{21})=10$ K] and partly by the disordering of the crystal structure responsible for superconductivity, since the defect cascades begin to overlap. J_c of TlGB8 plotted versus fluence shows a clear plateau in this fluence range, and an onset of this plateau is indicated for TlEK6b. Annealing experiments to recover the initial superconducting properties should lead to similar results as in Y-123 (Ref. 30) and are currently under way.

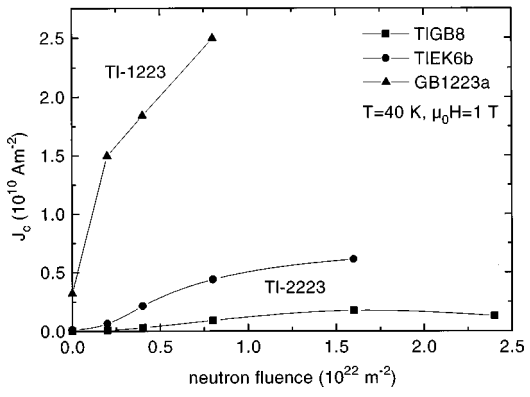

FIG. 12. J_c as a function of neutron fluence at 40 K and 1 T.

The results can be compared to Y-123 single crystals,[10] where, at 5 K and 2 T, $J_c\approx10^{11}$ A m^{-2} and, at 40 K and 2 T, $J_c\approx2.5\times10^{10}$ A m^{-2} were found after irradiation to 8×10^{21} m^{-2}. These values are somewhat higher than those for TlEK6b (at 2 T and 5 K, $\sim5\times10^{10}$ A m^{-2}; at 2 T and 40 K, $\sim1.3\times10^{9}$ A m^{-2}) and for GB1223a (at 40 K and 2 T, $\sim1.7\times10^{10}$ A m^{-2}) at the same fluence. However, the shift of the irreversibility line to higher fields and temperatures and thus the increase of the irreversible region are much more pronounced in the Tl-2223 system. In Y-123 the irreversibility point at 1 T was shifted from $t\approx0.93$ to 0.95 corresponding to about 1 K (Ref. 16) and in Tl-1223 from $t\approx0.78$ to 0.88 corresponding to about 6 K, but in Tl-2223 from $t\approx0.4$ to 0.65, corresponding to about 25 K.

Finally, we give an estimate of core pinning of pancakes by various defects in the unirradiated state and after the last irradiation step. The as-grown defect structure in Tl-2223 consists mainly of defects which act as weak pinning centers because of the low irreversibility line and the temperature dependence of J_c. The present defects are mainly point defects (diameter $<2\xi$) and a small number of larger defects (diameter $>2\xi$); strong pinning centers such as twin boundaries are absent. Because of the layered structure, the defects can act as pinning centers only if they are situated in the CuO_2 planes. The influence of magnetic pinning can be neglected since κ is very large. We assume first that the defects situated in the superconducting planes have a diameter of 2ξ or larger (but $\ll\lambda$) and can be approximated by disks with the thickness of one CuO_2layer ($\sim$0.3 nm), and second that larger defects with a similar diameter can be approximated by disks with the thickness of all three layers, i.e., $\sim$0.9 nm. The first type of disk-shaped defect should be able to pin one single pancake, the latter a stack of three pancakes. After irradiation, spherical defect cascades with a diameter of about 5 nm are created. Such a large defect can accommodate two stacks of CuO_2 planes on average. Contrary to Y-123, where the entire defect acts as a pinning center, only those parts of the defect containing CuO_2 planes are effective for pinning. A schematic drawing of these considerations is shown in Fig. 13. Using the $H_c(T)$ and $\xi(T)$ data of the previous section, we calculate the condensation energy for *one* pancake pinned by a thin disk-shaped defect and for a *stack* of three pancakes pinned by a thicker disk-shaped defect in the unirradiated state as well as for *two stacks* of pancakes pinned by a single defect cascade after the last irradiation step (16×10^{21} m^{-2}). This approach is useful at small applied fields, where ''isolated flux lines'' prevail, and provides us with information on the stability of the pinning wells, provided by these various defects, against thermal activation. The resulting condensation energy, therefore, represents an upper limit for the available pinning energy per defect site. The corresponding results are summarized in Fig. 14. We note that small defects (''1 pancake,'' ''1 stack'') are clearly weaker pinning centers in the irradiated state (solid lines) than before irradiation, because the intrinsic superconductive parameters of the material (H_c,ξ) have somewhat degraded. However, since their number is significantly enhanced (radiation-induced point defects and point defect clusters), they can certainly contribute to the J_c enhancement via collective pinning. Such a behavior has indeed been found experimentally in proton-irradiated Y-123 single

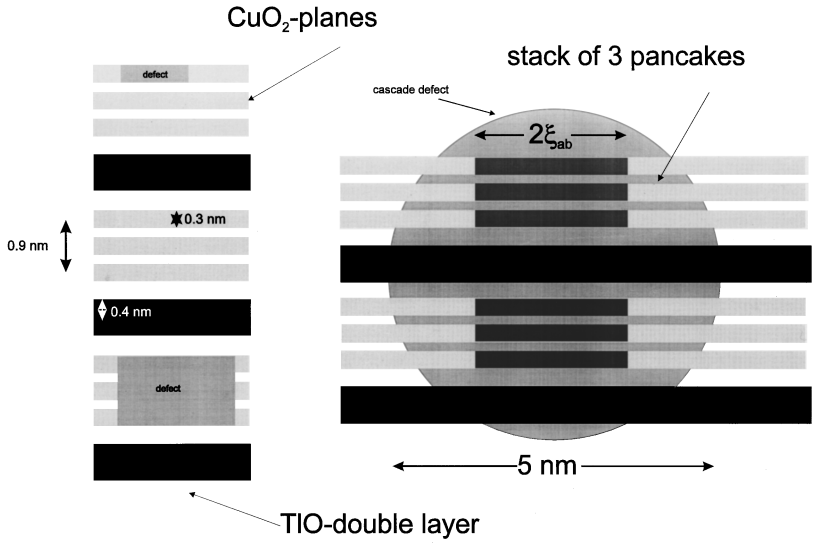

FIG. 13. Schematic drawing of disk-shaped pinning centers and stacks of pancakes pinned by a defect cascade.

crystals,[31] where almost no change or a slight degradation of the irreversibility line was observed, but the critical current densities were enhanced by the increased number of radiation-induced point defects. On the other hand, the defect cascades lead to strong pinning; i.e., the condensation energy crosses the thermal activation line only at ~90 K ($t \approx 0.8$), in good agreement with the results shown in Fig. 9. With regard to flux pinning in the unirradiated state, the data of Fig. 14 seem to suggest that most of the low-temperature pinning is caused by a mixture of smaller defects (''1 pancake'', ''1 stack''), since the dramatic increase of the irreversibility line occurs at around $t=0.4$ (where the condensation energy of the ''1 pancake'' defects crosses the thermal activation line), and pinning disappears at around $t \approx 0.7$, where the ''1 stack'' defects lose their pinning capability.

IV. SUMMARY

Tl-based single crystals with the nominal composition Tl-2223 and (TlPb)(SrBa)-1223 were investigated by SQUID magnetometry in the unirradiated state as well as after irradiation to cumulative fast neutron fluences up to 24×10^{21} m^{-2}. The basic mixed-state parameters were deduced from the reversible parts of $M(T)$ curves for Tl-2223. From a theory which takes thermally activated vortex fluctuations into account,[16] we calculated $\lambda(T)$ and $\mu_0 H_{c2}(T)$. Here $\lambda(T)$ was analyzed in terms of BCS theory, the two-fluid model, and within the framework of d-wave pairing. We find it impossible to finally decide between these temperature dependences, since their main differences occur only at low temperatures where no data are available due to the onset of flux pinning. However, the fit parameters do not match the theoretical exponents (0.5 in each case) and are clearly to small (0.27–0.35). This discrepancy could be related to the fact that the slope of $dM/d\ \ln H$ used for the derivation of the temperature dependence of the penetration depth was approximated linearly. Thus an average slope of the entire curve was used instead of the actual slope. Theories using the actual slope for the calculation of $\lambda(T)$ should result in a better agreement, at least for the correct temperature dependence. On the other hand, the upper critical field can be described by the BCS clean limit theory. The temperature dependence of the thermodynamic critical field was calculated in two different ways, which lead to almost identical results; and is also in excellent agreement with the BCS clean limit theory.

The critical current densities were obtained from M-H loops using an extended Bean model, which takes demagnetization effects into account. J_c in Tl-2223 is comparable to that of Y-123 at low temperatures ($T \leqslant 10$ K), but becomes negligibly small at about $T_c/3$. On the contrary, J_c in Tl-1223 shows a much weaker temperature dependence and remains significant up to 77 K. After neutron irradiation J_c is strongly enhanced in Tl-2223, whereas the increase is only moderate in Tl-1223. The irreversibility line of Tl-2223 has a very small initial slope, which rapidly increases below $t \approx 0.4$. Even after irradiation, this slope does not change very much, but the turning point to a rapid increase shifts to much

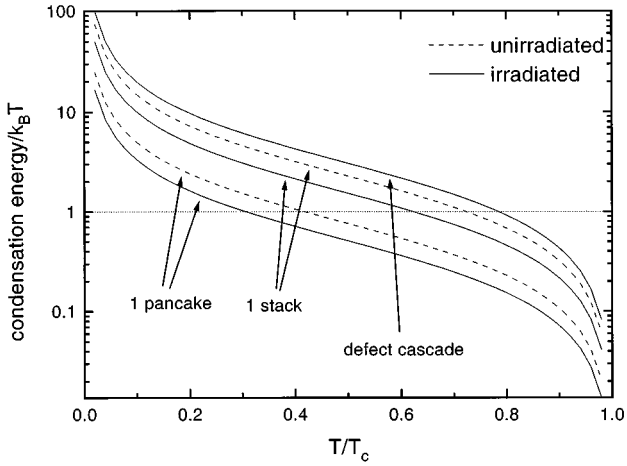

FIG. 14. Condensation energy pinning of pancakes. The condensation energy of disk-shaped pinning centers, $\mu_0 H_c^2(T)\pi\xi^2(T)q_z/2$, normalized by the thermal energy $k_B T$ is plotted vs reduced temperature $t=T/T_c$. The defect volumes (cf. Fig. 13) are calculated from the experimentally determined data for $H_c(T)$ and $\xi(T)$, and q_z is 0.3 nm (''1 pancake''), 0.9 nm (''1 stack''), and 1.8 nm (''defect cascade''), i.e., the maximum number of pancakes fitting into the cascade volume. Dashed line, unirradiated; solid line, irradiated to 16×10^{21} m^{-2} ($E>0.1$ MeV).

higher temperatures. In Tl-1223, the shift of the irreversibility line to higher temperatures and fields is only moderate, but the functional dependence of $H_{\rm irr}(T)$ changes from exponential to a power law.

Because of the layered structure of Tl-2223, the magnetic microstructure consists of correlated stacks of pancakes, which are coupled by magnetic interactions at low temperatures. However, they decouple at higher temperatures, which requires individual pinning of each pancake. The distance between the copper oxide planes is much shorter in Tl-1223, similar to Y-123. Consequently, the behavior is more 3D; i.e., high critical current densities are found up to elevated temperatures and the irreversible region is large. After irradiation, the enhancement of J_c is not very pronounced in both compounds at low temperatures, which indicates that the pinning behavior is nearly unchanged. However, at higher temperatures the increase is tremendous, in particular in Tl-2223, and large J_c's are found at fields and temperatures where complete reversibility prevailed before irradiation. This occurs at temperatures where the correlated stacks of pancakes have already decoupled. Thus defect cascades are strong pinning centers also for pancakes. This conclusion is supported by condensation energy considerations.

ACKNOWLEDGMENTS

Valuable technical support by H. Niedermaier is gratefully acknowledged. We would like to thank Professor W. Y. Liang (Cambridge) and Dr. F. Ladenberger (Göttingen) for supplying the single crystals and Dr. V. Kogan (Ames) for valuable discussions. This work was supported in part by Fonds zur Förderung der Wissenschaftlichen Forschung, Vienna, under Contract No. 9194 and by the EU Brite Euram program under Contract No. BRE2-CT93-0531.

[1] J. G. Bednorz and K. A. Müller, Z. Phys. B **64**, 189 (1986).
[2] Z. Z. Sheng and A. M. Hermann, Nature **332**, 55 (1988); R. M. Hazen, in *Properties of High Temperature Superconductors*, edited by D. Ginsberg (World Scientific, Singapore, 1990), Pt. II, p. 121.
[3] H. W. Weber and G. W. Crabtree, in *Studies of High-Temperature Superconductors*, edited by A. V. Narlikar (Nova Science, New York, 1991), Vol. 9, p. 35; L. Civale, A. D. Marwick, T. K. Worthington, M. A. Kirk, J. R. Thompson, L. Krusin-Elbaum, Y. Sun, R. Clem, and F. Holtzberg, Phys. Rev. Lett. **67**, 648 (1991).
[4] M. C. Frischherz, M. A. Kirk, J. Farmer, L. R. Greenwood, and H. W. Weber, Physica C **232**, 309 (1994).
[5] M. Aleksa, Ph.D. thesis, Technical University of Vienna, 1996.
[6] G. Brandstätter, F. M. Sauerzopf, H. W. Weber, W. Mexner, H. C. Freyhardt, A. Aghaei, F. Ladenberger, and E. Schwarzmann, in *Applied Superconductivity*, edited by H. C. Freyhardt (DGM Informationsges-Verlag, Obervrsel, 1993), p. 109; K. Winzer, Ann. Phys. (Leipzig) **1**, 479 (1992); K. Aihara, T. Doi, A. Soeto, S. Takeuchi, T. Yuasa, M. S. Eido, T. Kamo, and S. Matsuda, Cryogenics **32**, 936 (1992).
[7] H. W. Weber, H. Böck, E. Unfried, and L. R. Greenwood, J. Nucl. Mater. **137**, 236 (1986).
[8] J. R. Thompson, J. G. Ossandon, D. K. Christen, B. C. Chakoumakos, Y. RenSun, M. Paranthaman, and J. Brynestad, Phys. Rev. B **48** 14 031 (1993).
[9] X. M. Yang and G. Brandstätter (unpublished).
[10] F. M. Sauerzopf, H. P. Wiesinger, H. W. Weber, and G. W. Crabtree, Phys. Rev. B **51**, 6002 (1995).
[11] P. H. Kes, C. J. van der Beek, M. P. Maley, and M. E. McHenry, Phys. Rev. Lett. **62**, 1908 (1989).
[12] A. E. Koshelev, Phys. Rev. B **50**, 506 (1994); L. N. Bulaevskii, M. Ledvij, and V. G. Kogan, Phys. Rev. Lett. **68**, 3773 (1992).
[13] X. L. Wang, X. M. Yang, H. W. Weber, R. Abraham, K. Lebbou, M. Th. Cohen-Adad, E. Halwax, and P. Wiede, J. Cryst. Growth **167**, 93 (1996).
[14] J. R. Clem, Phys. Rev. B **43**, 7837 (1991); Z. Hao, J. R. Clem, M. W. McElfresh, L. Civale, A. P. Malozemoff, and F. Holtzberg, *ibid*. **43**, 2844 (1991); V. G. Kogan, M. Ledvij, A. Y. Simonov, J. H. Cho, and D. C. Johnston, Phys. Rev. Lett. **70**, 1870 (1993).
[15] A. E. Koshelev, Phys. Rev. B **50**, 506 (1994).
[16] L. N. Bulaevskii, M. Ledvij, and V. G. Kogan, Phys. Rev. Lett. **68**, 3773 (1992).
[17] K. H. Fischer, Physica C **210**, 179 (1993).
[18] L. N. Bulaevskii, M. P. Maley, and J. H. Cho (unpublished).
[19] J. C. Martinez, P. J. E. M. van der Linden, L. N. Bulaevskii, S. Brongersma, A. Koshelev, J. A. A. J. Perenboom, A. A. Menovsky, and P. H. Kes, Phys. Rev. Lett. **72**, 3614 (1994).
[20] E. Helfand and N. R. Werthamer, Phys. Rev. **147**, 288 (1966).
[21] B. Mühlschlegel, Z. Phys. **155**, 313 (1959).
[22] A. Junod, K. Q. Wang, G. Triscone, C. Opagiste, M. Couach, A. F. Khoder, and J. Müller, J. Alloys Compd. **195**, 547 (1993).
[23] A. Junod, K. Q. Wang, T. Tsukamoto, G. Triscone, B. Revaz, E. Walker, and J. Müller, Physica C **229**, 209 (1994).
[24] H. P. Wiesinger, F. M. Sauerzopf, and H. W. Weber, Physica C **203**, 121 (1992).
[25] H. P. Wiesinger, F. M. Sauerzopf, H. W. Weber, H. Gerstenberg, and G. W. Crabtree, Europhys. Lett. **20**, 541 (1992).
[26] M. Däumling, J. M. Seuntjas, and D. C. Larbalestier, Nature **346**, 332 (1990).
[27] M. C. Frischherz, F. M. Sauerzopf, H. W. Weber, M. Murakami, and G. A. Emel'chenko, Supercond. Sci. Technol. **8**, 485 (1995); M. Suenaga, D. O. Welch, and R. Budhani, *ibid*. **5**, 3 (1992).
[28] F. M. Sauerzopf, H. P. Wiesinger, H. W. Weber, and G. W. Crabtree, Adv. Cryog. Eng. **38**, 901 (1992).
[29] V. V. Metlushko, G. Güntherodt, V. V. Moshchalkov, Y. Bruynseraede, H. Thomas, and K. Winzer, in *Applied Superconductivity* (Ref. 6), p. 853.
[30] B. M. Vlcek, M. C. Frischherz, S. Fleshler, U. Welp, J. Z. Liu, J. Downey, K. G. Vandervoort, G. W. Crabtree, M. A. Kirk, J. Giapintzakis, and J. Farmer, Phys. Rev. B **46**, 6441 (1992); B. M. Vlcek, H. K. Viswanathan, M. C. Frischherz, S. Fleshler, K. Vandervoort, J. Downey, U. Welp, M. A. Kirk, and G. W. Crabtree, *ibid*. **48**, 4067 (1993).
[31] L. Civale, A. D. Marwick, M. W. McElfresh, T. K. Worthington, A. P. Malozemoff, F. H. Holtzberg, J. R. Thompson, and M. A. Kirk, Phys. Rev. Lett. **65**, 1164 (1990).